Dopamine-Assisted Synthesis of Carbon-Coated Silica for PCR Enhancement

Ji Young Park,[†] Seung Hun Back,[†] Sung-Jin Chang,[†] Seok Jae Lee,[‡] Kyoung G. Lee,*,[‡] and Tae Jung Park*,[†]

[†]Department of Chemistry, Chung-Ang University, 84 Heukseok-ro, Dongjak-gu, Seoul 156-756, Republic of Korea
[‡]National Nanofab Center, 291 Daehak-ro, Yuseong-gu, Daejeon 305-806, Republic of Korea

Ⓢ *Supporting Information*

ABSTRACT: Polymerase chain reaction (PCR) has become one of the most popular methods to identify genomic information on cells and tissues as well as to solve crimes and check genetic diseases. Recently, the nanomaterials including nanocomposite and nanoparticles have been considered as a next generation of solution to improve both quality and productivity of PCR. Herein, taking into these demands, carbon-coated silica was synthesized using silica particles via polymerization of biocompatible dopamine (PD) to form polydopamine (PDA) film and carbonization of PDA into graphitic structures. For further investigation of the effects of as-prepared silica, PDA-coated silica (PDA silica), and carbonized PDA silica (C-PDA silica), two different types of genes were adopted to investigate the influences of them in the PCR. Furthermore, the strong interaction between the nanocomposites and PCR reagents including polymerase and primers enables regulation of the PCR performance. The effectiveness of the nanocomposites was also confirmed through adopting the conventional PCR and real-time PCR with two different types of DNA as realistic models and different kinds of analytical methods. These findings could provide helpful insight for the potential application in biosensors and biomedical diagnosis.

KEYWORDS: silica, polydopamine, polymerase chain reaction, nanocomposite, PCR enhancer
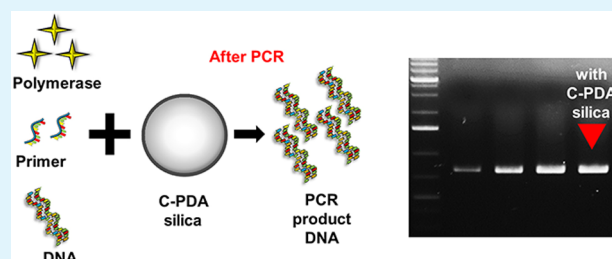
1. INTRODUCTION

A rapid and accurate way to identify genomic information is the most essential process to biological systems due to its unique characteristics and potential applications in biomedical fields[1] such as in diagnosis[2] and in biosensors.[3,4] Among the numerous methods of DNA analysis, polymerase chain reaction (PCR) is a sensitive technique that enables rapid amplification of a specific DNA segment. Only trace amounts of DNA are needed for PCR to generate millions to billions of copies of a specific DNA fragment or gene in tens of seconds, which allows detection and identification of gene sequences and quantitative measurements of gene expression. Because of its simplicity and reliability, PCR is popular, commonly used in medical and biological research for DNA sequencing, gene cloning, and pathogen detection.[5−7] Although PCR is still a powerful method to amplify specific genes, the critical drawbacks of PCR such as an error-prone reaction could not be overcome due to its *in vitro* conditions. Accuracy, sensitivity, and the PCR product size and length limitation openly lead to the inevitable issues in fidelity and efficiency of PCR.[8]

Recently, nanomaterial-assisted PCR (or nano-PCR) has also become popular because it utilizes nanomaterials to enhance PCR efficiency.[9] Various types of nanomaterials have been used as PCR enhancers such as gold nanoparticles,[10,11] quantum dots,[12,13] and carbon-based materials such as fullerenes,[14]

graphene oxide (GO), reduced graphene oxide (rGO),[15,16] and carbon nanotubes (CNTs).[17−19] The nanomaterials provide exceptional physical and chemical properties such as large surface area and volume ratio, heat transfer rate,[20−23] and potential binding sites[24,25] for biological materials. Especially, carbon-based materials with graphitic structure exhibit a high thermal conductivity, weak van der Waals coupling, and $\pi-\pi$ interaction[26] which can affect enhancement of PCR.[9] In spite of the capabilities and merits of carbon-based materials in PCR technology, a serious level of agglomeration inevitably reduces the material's surface area and the performance of PCR.[27]

To overcome such challenges, carbon and silica-based nanocomposites (i.e., inorganic/organic hybrid composites) have provided an alternative choice to meet the requirements. The nanocomposite adopts the advantages such as mechanical and chemical properties of the inorganic material and the organic polymer. Up to now, monodispersed silica has presented a high biocompatibility and suitability for biological applications.[28−30] However, the strong negatively charged silica particles openly require extra surface modifications. Another well-known polydopamine (PDA) is also inexpensive and a

Table 1. Oligonucleotide Sequences for PCR Amplification Used in This Study

target gene	size (bp)	sequences (5′-3′)	template
egfp	800	F: AAAATTCCATATGGTGAGCAAGGGCGA	pEGFP-C1
		R: TTCTAAGCTTTTACTTGTACAGCTCGTC	
eae1	248	F: ATGCTTAGTGCTGGTTTAGG	genomic DNA of *E. coli* NCCP 13715
		R: GCCTTCATCATTTCGCTTTC	

biocompatible material that is commonly found from mussel adhesive protein.[31,32] Additionally, biofriendly and bioadhesive PDA enables binding over a universal surface via the oxidative self-polymerization of dopamine (i.e., monomer) at basic pH condition. Because PDA provides a carbon source as an adhesion layer, this can be immobilized together on the one place of biomolecules. This is a key factor of enhancing the stability of DNA polymerase and yield of PCR product. Moreover, the carbonization of PDA allows the formation of graphene-like structures and provides nitrogen (N)-doping effect to adopt the benefits of N-doped and carbon-based ordered structures for PCR enhancement.[33,34]

Herein, we develop a simple and green chemical method to prepare C-PDA silica and employ them as a PCR enhancer. The silica particle as a core substrate and PDA as a biofriendly material were used to form thin carbon layers surrounding silica. After pyrolysis of PDA, the heterogeneous PDA structures convert into fairly ordered multilayered carbon structures which are similar to the graphene-like structures.[35,36] The chemical structural similarity of as-prepared carbon-coated silica allows us to adopt the advantages of carbon-based materials. We further investigate the interaction between PCR reagents and individual components of C-PDA silica by employing as-prepared silica and PDA silica during PCR. Moreover, the effectiveness of these nanocomposites was further demonstrated using the conventional and real-time PCR with two different types of DNA as realistic models and different kinds of analytical methods.

2. EXPERIMENTAL SECTION

2.1. Materials. Tetraethylorthsilicate (TEOS) (98%), ammonium hydroxide (28−29%), ethanol (99.5%), dopamine (DA) hydrochloride, and tris(hydroxymethyl)aminomethane (TRIS) were purchased from Sigma-Aldrich (St. Louis, MO, USA). MAXIME PCR premix kit and DNA purification kit were purchased from iNtRON Biotechnology (Seongnam, Korea). Deionized (DI) water from water purification equipment (Direct-Q 3 Water Purification System, Millipore, Billerica, MA, USA) was used in this study.

2.2. Synthesis of Silica. Silica particles were synthesized using the Stöber method.[37] First, the solution mixed with 250 mL of ethanol and 8.7 mL of DI water was added to TEOS and ammonium hydroxide solution by stirring with a magnetic bar. The mixture was gently stirred for 3 h and subsequently centrifuged. Then, the mixture was washed several times using ethanol and water, respectively. The finally obtained white suspension was dried overnight in a vacuum oven at 60 °C.

2.3. Formation of Polydopamine on Silica. A 100 mg amount of silica was dispersed in Tris buffer (10 mM, pH 8.5) at 25 °C using sonication for 30 min. DA hydrochloride was mixed in the solution (2 mg/mL) and then stirred with centrifugation at room temperature for 6 h. After the reaction was over, the brown-colored composites were centrifuged to separate the precipitate. The precipitate was carefully washed with DI water several times to remove unreacted PDA.

2.4. Carbonization of Polydopamine on Silica. The PDA silica was converted into carbonized PDA (C-PDA) silica through a heating procedure. The PDA silica was placed in the vacuum oven under N₂ atmosphere at a heating rate of 1 °C/min from room temperature to 450 °C, and the temperature was then maintained at 450 °C for 6 h.

2.5. Characterization. To understand the morphology and surface modification of the synthesized particles, a 200 kV field-emission transmission electron microscope (FE-TEM; JEM-2100F, Jeol, Tokyo, Japan) and field-emission scanning electron microscope (FE-SEM; S-4800, Hitachi, Tokyo, Japan) were used. Structural properties were analyzed by Fourier transform infrared (FT-IR) spectroscopy (IFS6v/S, Bruker, Karlsruhe, Germany) and Raman spectroscopy (NTEGRA spectra, NT-MDT, Moscow, Russia).

2.6. Preparation of Different Types of Composites for PCR. As-prepared silica, PDA silica, and C-PDA silica were separately suspended in autoclaved DI water. To prepare the well-dispersed solution, each mixture (1 mg/mL) was placed in a water bath and sonicated with a frequency of 40 kHz and ultrasonic power of 100 W for 30 min. After the sonication, all of the mixtures were carefully diluted to 10^{-3} μg/mL. In order to ensure proper mixing and prevent aggregation among nanomaterials, the sonication step was followed by dilution steps. Two different types of PCR templates were purified from *Escherichia coli* (*E. coli*) genomic DNA and plasmid DNA, respectively.

2.7. Conventional PCR Methodologies. All experiments were performed using a PCR machine (T100 Thermal cycler, Biorad, Hercules, CA, USA) with premixed solution. Specific primers for amplification from pEGFP-C1 and the genomic DNA of *E. coli* (*Escherichia coli* NCCP 13715 obtained from the the Korean Food and Drug Administration) were used as shown in Table 1. The PCR reaction mixture was composed with the following final concentrations; i-*Taq* DNA polymerase of 2.5 U/μL in the reaction buffer, dNTP of 2.5 mM, 1X reaction buffer, and 1X gel-loading buffer. In this reaction mixture, a template DNA of 1 μL, forward and reverse primers of 10 pmol each, and with or without nanomaterials in total volume of 20 μL were added. The PCR amplification was performed by the following procedures. The PCR process for the initial denaturation was gradually increased until 94 °C for 5 min. Sequentially, temperature was gradually increased to 94 °C for denaturation (step 1) for 30 s. Annealing (step 2) was cooled to 50 °C for 30 s. Extension (step 3) at 72 °C for 50 s was started for the synthesis of the specific DNA sequence (30 cycles). The PCR products were implemented using electrophoresis (Mupid-2 plus, Advance, Tokyo, Japan) using 0.8% (w/v) agarose gel (Seakem LE agarose, Lonza, Basel, Switzerland). The molecular weight marker for *E. coli* (100 bp DNA ladder; Bioneer, Daejeon, Korea) and marker for pEGFP-C1 (1 kb plus; Accugen Healthcare, Daejeon, Korea) were used in order to determine the DNA size. Finally, the performance of the nanomaterials for amplification and analysis of products was confirmed via the band intensities using a compact gel documentation system (Slite 140S, Avegene, New Taipei, Taiwan).

2.8. Real-Time PCR Amplification. For each real-time PCR, SYBR green solution (SYBR Premix Ex *Taq*II, Takara Bio, Shiga, Japan) was used with the components as follows: *Takara Ex Taq* HS, dNTP Mixture, Mg²⁺, Tli RNaseH, and SYBR Green I. Genomic DNA of *E. coli* was used as a template with forward and reverse primers of 10 pmol for the reaction and with or without nanomaterials in a total volume of 25 μL. Like conventional PCR method, the real-time PCR was performed with two steps using a real-time PCR machine (CFX96, Biorad). Temperature was gradually increased until 95 °C for 3 min for the initial denaturation step and then maintained at 94 °C for 10 s (step 1). Annealing (step 2) to 50 °C for 30 s was cooled. The two steps were repeated with 40 cycles. After the reaction, a dissociation step was executed for checking the melting curves of PCR amplification. Finally, the CFX manager from Biorad software was

used to quantify the PCR products and their temperature melting curves.

3. RESULTS AND DISCUSSION

3.1. Preparation and Characterization of Nanocomposites. Overall synthesis processes of silica, PDA silica, and C-PDA silica are depicted in Figure 1a. The synthesis was
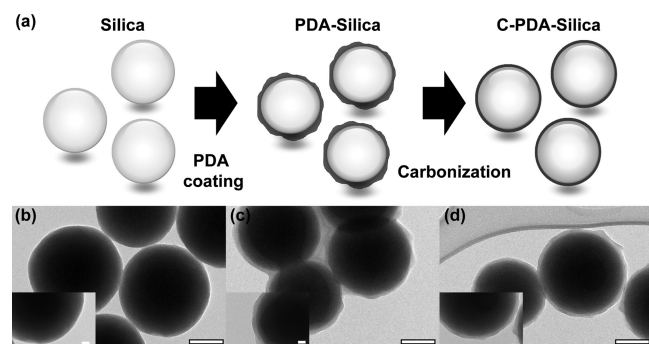

Figure 1. (a) Schematic illustration of the synthesis process of silica, PDA silica, and C-PDA silica and (b) their corresponding TEM images. All scale bars in b−d are 100 nm for the main panels and 20 nm for the insets, respectively.

mainly composed of a three-part process as follows: (1) formation of silica particles, (2) PDA coating over the surface of silica, and (3) carbonization of PDA silica (see Experimental Sections 2.2−2.4.). As shown in Supporting Information Figure S1 and Figure 1b, the monodispersed as-prepared silica particles exhibited an average diameter of 271 ± 5.5 nm and their surface was smooth. After PDA coating, the thin PDA film was uniformly covered all over the silica and its average thickness was 12.6 ± 1.4 nm (Figure 1c). On the other hand, an average thickness of the C-PDA film on the silica was 7.91 ± 0.4 nm (Figure 1d), indicating that the thermal carbonization of the PDA film on the silica significantly reduced its thickness. Moreover, the C-PDA film became smoother in comparison with the PDA film.

As-prepared silica, PDA silica, and C-PDA silica were further investigated with FT-IR and Raman spectroscopies to confirm their chemical compositions and structural properties (Figure 2). The typical FT-IR spectra of as-prepared silica, PDA silica, and C-PDA silica, as indicated by black, red, and blue traces, respectively (Figure 2a), commonly showed three prominent absorption bands at 475, 810, and 1113 cm^{-1}. These three bands correspond to a part of the transverse-optical (TO)
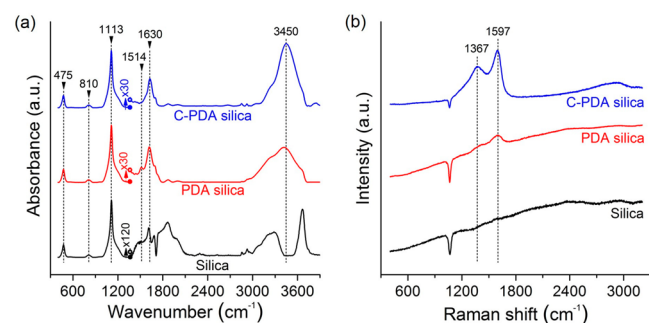

Figure 2. (a) FT-IR spectra of silica (black), PDA silica (red), and C-PDA silica (blue). (b) Raman spectra of silica (black), PDA silica (red), and C-PDA silica (blue).

vibrational modes of the Si−O−Si linkage in silica (or combinations of vibrations of the silica network), confirming the existence of silica together with the results of elemental mapping (Figure S2 in the Supporting Information) and are referred to as TO_1, TO_2, and TO_3, respectively. In particular, TO_1, TO_2, and TO_3 are due to the perpendicular motions of the bridging oxygen to the Si−O−Si plane (the rocking mode), the stretching of oxygen atoms along the bisecting line of the Si−O−Si (the symmetric mode), and the motion in opposite distortion of the two neighboring Si−O bonds (the antisymmetric mode), respectively.[38] It is worth noting that the weak peak at 3668 cm^{-1} in the FT-IR spectrum of the as-prepared silica is attributed to silanols which are perturbed by interparticle contact.[39] In contrast to the FT-IR spectra, no obvious evidence for the existence of silica is obtained from the Raman spectra of as-prepared silica, PDA silica, and C-PDA silica, as presented by black, red, and blue traces, respectively (Figure 2b).

In contrast to the as-prepared silica, the FT-IR spectra of the PDA silica and the C-PDA silica showed a newly developed broad band at 3450 cm^{-1}, corresponding to the N−H stretching mode of secondary amine.[40] It should be emphasized that , in the FT-IR spectrum of the as-prepared silica, the broad band due to the O−H stretching vibrations in the region between 3000 and 3400 cm^{-1} clearly emerge, while no band at 3450 cm^{-1} corresponding to the N−H stretching vibrations is discernible. In addition, the peak intensity at 3450 cm^{-1} is relatively stronger than intensities in the range of 3000−3400 cm^{-1} in the FT-IR spectra of the PDA silica and the C-PDA silica, implying that two such types of stretching modes are distinguishable in our samples. Moreover, the Raman spectra of the PDA silica (Figure 2b, red trace) and the C-PDA silica (Figure 2b, blue trace) exhibited two distinctive bands at approximately 1367 and 1597 cm^{-1}, corresponding to the D and G bands, respectively, whereas the Raman spectrum of the as-prepared silica did not display these two bands. The D band is due to the A_{1g} breathing mode of the sp^3 carbon, and the G band is assigned to the in-plane bond stretching of all pairs of sp^2 carbon atoms in both rings and chains.[41] Together with the results of elemental mapping (Figure S2 in the Supporting Information), these FT-IR and Raman results confirmed the formation of thin PDA layers on the silica.

The Raman spectrum of the C-PDA silica showed the D and G bands more strongly compared with that of the PDA silica. In addition, the Raman spectrum of the C-PDA silica also showed a discernible band in the range between 2650 and 3000 cm^{-1}, corresponding to typical positions of the 2D band in defective graphene.[42,43] The 2D band is associated with the breathing modes of six-atom rings.[44] These imply that carbonization of the PDA silica induced restoration of graphitic structure in the PDA silica. Furthermore, a weak band at 1514 cm^{-1}, attributed to the N−H bending mode of aromatic secondary amine,[40] appears only in the FTIR spectrum of the PDA silica, indicating further modification of the PDA silica as well as graphitization by the carbonization of the PDA silica.

3.2. Enhancement of PCR Performance. PCR performances of as-prepared silica, PDA silica, and C-PDA silica were investigated using agarose gel electrophoresis with two types of DNA, genomic DNA of *E. coli* (*eae1*, 248 bp) and pEGFP-C1 plasmid (*egfp*, 800 bp) as shown in Figure 3. The PCR results without nanomaterials (the positive controls) in lane 1 were comparted with those of silica (lane 2), PDA silica (lane 3), and C-PDA silica (lane 4), and it is also presented in Figure 3a,b. All
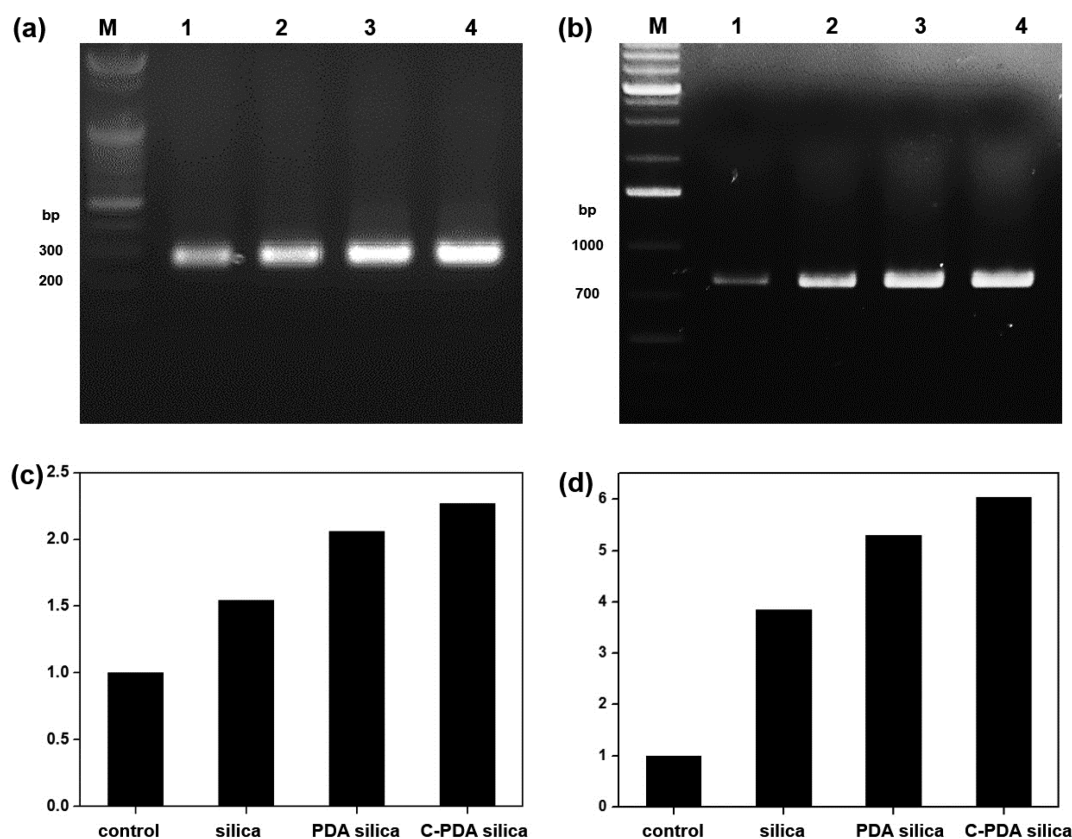
Figure 3. Agarose gel electrophoresis for analyzing the concentration of PCR products obtained from two different templates, (a) the genomic DNA of *E. coli* (*eael*; size, 248 bp) and (b) pEGFP-C1 plasmid (*egfp*; size, 800 bp), (c) the DNA band intensities of the gel images from (a) the *E. coli* genomic DNA and (d) the pEGFP-C1 quantified with the Quantity One program from Biorad: lane M, DNA marker; lane 1, control; lane 2, silica-assisted PCR; lane 3, PDA silica-assisted PCR; lane 4, C-PDA silica-assisted PCR. All of the added nanomaterials were 2.5 pg/μL.

of the amounts of PCR products were increased when the silica, PDA silica, and C-PDA silica were utilized in comparison with that of PCR products of the positive controls regardless of the size of the DNA, as shown in Figure 3a,b. For clarity, the band intensities at *eael* (Figure 3c) and *egfp* (Figure 3d), which reflect the concentrations of PCR products, were obtained from the images of agarose gel electrophoresis in Figure 3a,b, respectively. For convenience, the band intensities in Figure 3c,d were normalized by the band intensities of PCR products of the corresponding positive controls, respectively. In particular, the concentrations of PCR products of the *E. coli* genomic DNA with as-prepared silica, PDA silica, and C-PDA silica were about 1.5, 2.0, and 2.2 times higher than that of PCR product of the positive control, respectively (Figure 3c). In addition, the concentrations of PCR products of the pEGFP-C1 plasmid with as-prepared silica, PDA silica, and C-PDA silica were also about 3.8, 5.3, and 6.0 times higher than that of PCR product of the positive control, respectively (Figure 3d). These results exhibited that both the yield and the efficiency of the PCR reaction with C-PDA silica were much higher than those of the PCR reaction with silica and PDA silica. From these results, it could be suggested that the C-PDA- and silica-based nanocomposites enhance the PCR performance in both the short and long DNAs.

The effects of silica, PDA silica, and C-PDA silica on the PCR were also investigated by employing real-time PCR (Figure 4) as simultaneously quantifying the fluorescent intensity changes during amplification of the target DNA. In this case, the relative fluorescence unit (RFU) is directly

associated with the yield of PCR products as responding to the nanocomposites (Figure 4a,b). As compared to the control, all of the PCR efficiencies of both *eael* and *egfp* were enhanced with the presence of nanocomposites. Among them, the C-PDA silica also presented the best efficiency of the real-time PCR compared with others. In particular, the efficiency of the C-PDA silica is about 1.5 and 1.2 times higher than those of silica and PDA-silica, respectively (Figure 4c,d). These results demonstrated that the C-PDA silica was the most efficient for the PCR processes. Especially, the PCR products from the *egfp* sequence could be amplified with large amounts of DNAs compared with the results of the short DNA sequence. Thus, it could be suggested that the long DNA sequence can be affected more by efficient PCR performance using the nanocomposites than the *eael* sequence (i.e., relatively short size) due to the specific and strong binding of primers to the template DNAs. Moreover, both conventional PCR and real-time PCR exhibited similar enhancement of PCR efficiency, and these results also proved that the nanocomposites can not only reduce the PCR cycle but also increase the final quantity of the PCR product.

Annealing temperature is a critical parameter in the PCR step, and thus the inspection of a broad range of annealing temperatures is highly required to enhance both efficiency and accuracy of PCR. To examine the effects of the annealing temperature on nanomaterials-assisted PCR performance, PCR performances of silica, PDA silica, and C-PDA silica were separately tested only with the genomic DNA of *E. coli* in the range of annealing temperatures from 40 to 55 °C. The final PCR products were analyzed using gel electrophoresis as shown
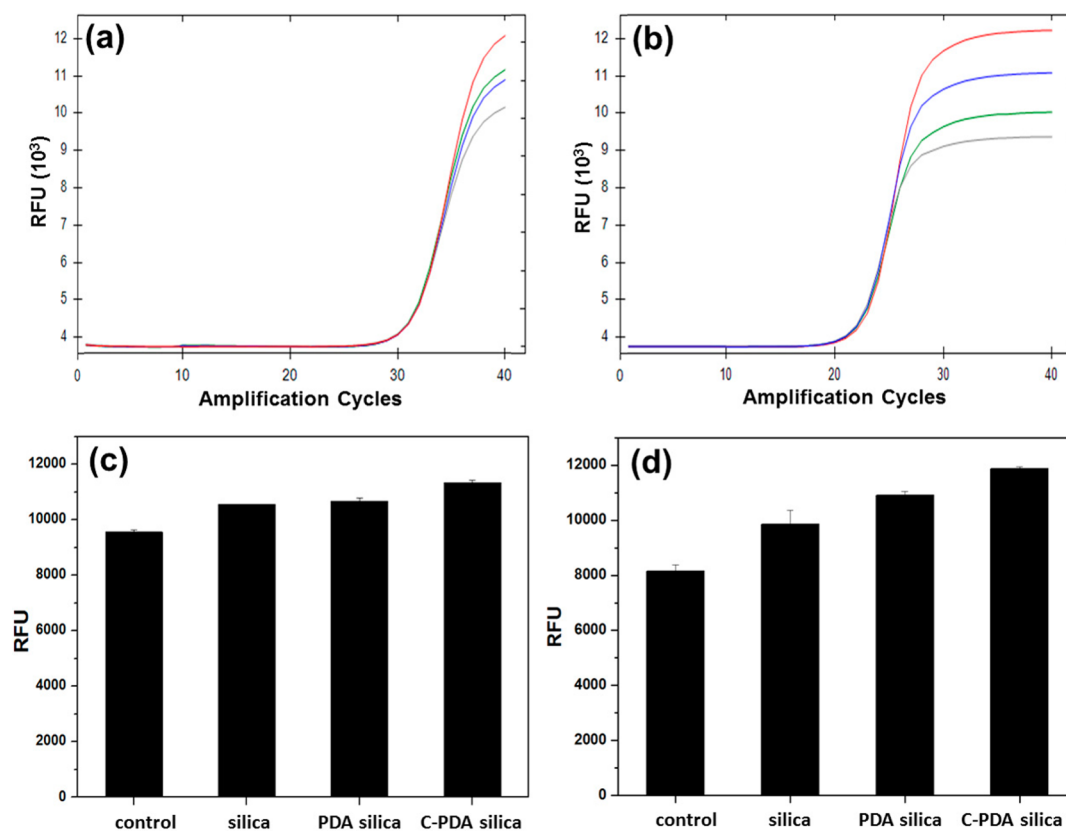
Figure 4. Efficiency of PCR amplification for primer eae1 using *E. coli* genomic DNA and pEGFP-C1 as templates. Amplification plots for real-time PCR assays using nanomaterials for (a) eael and (b) pEGFP-C1, respectively. Graphs showing fluorescent intensities after real-time PCR of (c) eael and (d) pEGFP-C1, respectively.
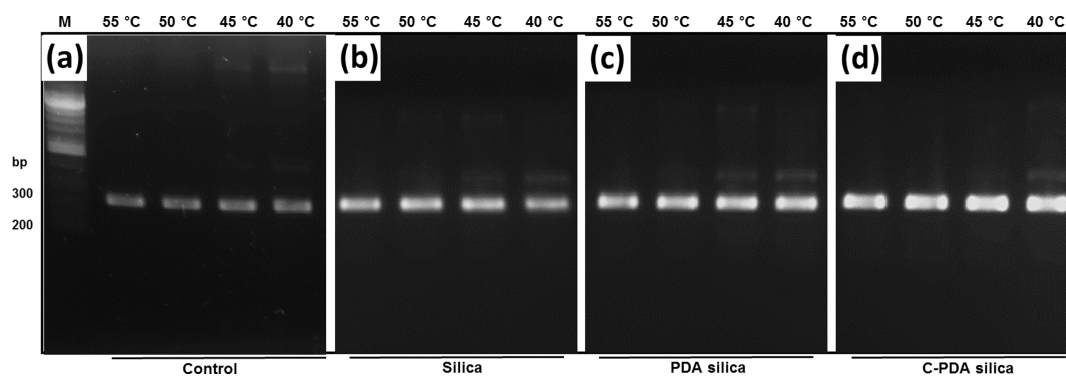

Figure 5. Effect of the annealing temperature on the efficiency of the PCR using genomic DNA of *E. coli*: (a) control without nanocomposites; (b) silica-assisted PCR; (c) PDA silica-assisted PCR; (d) C-PDA silica-assisted PCR. Lane M, DNA marker; lanes 1−4, annealing temperature from 55 to 40 °C. Each concentration of nanomaterials was 2.5 pg/μL.

in Figure 5. PDA-based composites showed yield improvement at the broad range of annealing temperatures (40−55 °C). The results indicated that nanocomposite-assisted PCR guarantees the improvement of PCR performance in the broad ranges of the annealing temperature.

3.3. Role of Nanocomposites in the PCR. Previously, it has been reported that ssDNA, DNA, and DNA polymerase could bind on the nanomaterial surface. However, limited materials such as carbon nanotubes, graphene, and gold have been studied so far. In order to understand the role of the silica, PDA-silica, and C-PDA silica during the PCR, we hypothesized the chemical interaction between the surface of nanocomposites and PCR components such as primers and

polymerase. The DNA polymerase had different degrees of adsorption to the silica, PDA silica, and C-PDA silica via polar groups in their amino acid structures. To investigate the effects, the individual particles (i.e., silica, PDA silica, and C-PDA silica) were carefully mixed with the following components, (1) polymerase, (2) primers, and (3) both primers and polymerase. After the reaction, the size differences of those composites were measured using dynamic light scattering (DLS) method shown in Figure 6a. After reacting with the primer, polymerase, and both primer and polymerase with as-prepared silica, PDA-silica, and C-PDA silica, the sizes of both PDA-silica and C-PDA silica were increased while the pristine silica remained almost the same size (Figure 6a). These phenomena could be understood
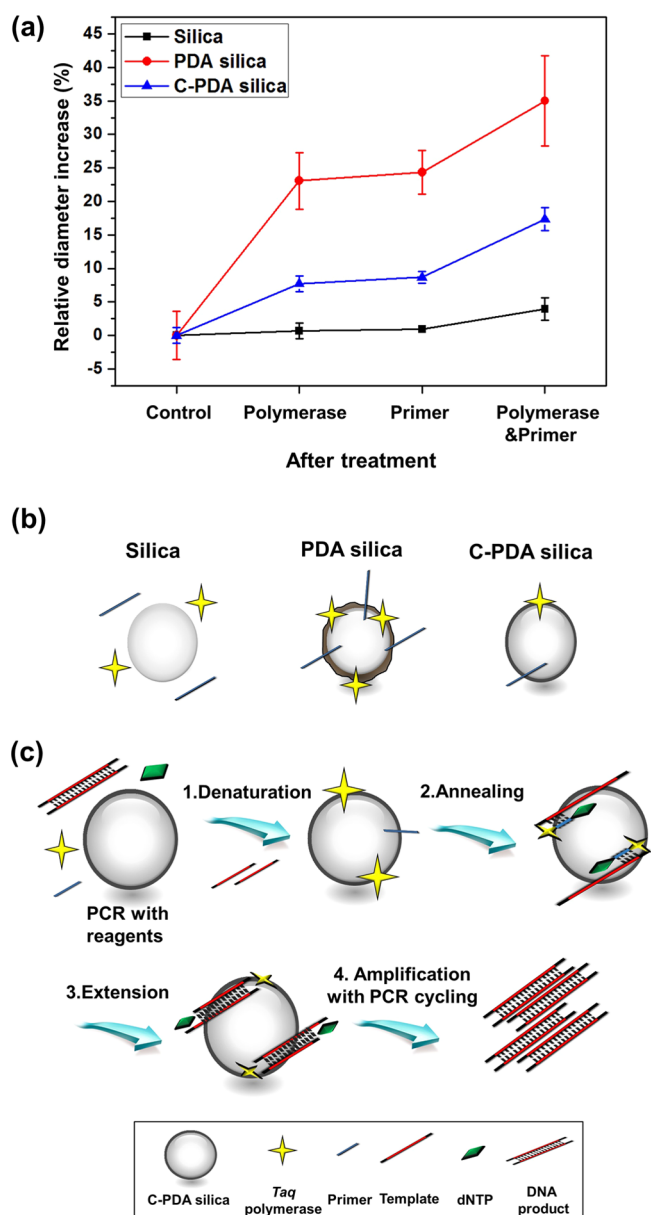
Figure 6. Thickness changes of silica, PDA silica, and C-PDA silica by DLS particle size analysis (a) and the schematic illustration for the proposed mechanism of (b) interaction of primer, polymerase, and nanocomposites, and (c) C-PDA silica in the PCR process.

from surface characteristic differences of the particles. The minor diameter changes of silica after mixing with primers or/and polymers were mainly attributed to a strong negative surface charge, which prevented a strongly negatively charged DNA or PCR component from adhering to the silica surface (black line in Figure 6a). Compared to the silica, the diameter of PDA silica was slightly increased about 20−32% (red line in Figure 6a). The strong adsorptions of polymerase and primer to the PDA silica were attributed to the catechol and quinone groups of PDA. By contrast, the C-PDA showed moderate interaction with polymerase or/and primer compared with the PDA results. In particular, the diameter of the C-PDA silica was slightly increased about 5−15% (blue line in Figure 6a). After carbonization of PDA, the main structures would be somewhat similar to the graphitic structures but the different surface characteristics can be expected from N-doped carbon from

carbonization of PDA.[33] The plausible binding activities between nanocomposites and PCR reagents such as primers and polymerase are illustrated as shown in Figure 6b. These different binding capabilities are attributed to different PCR performances as shown in Figure 4. Although the PDA silica provided the strongest adsorption of the primer and polymerase, the mild condition for the immobilization of polymerase and primer (i.e., C-PDA silica) gave the best PCR performance. The proposed processes in the PCR with C-PDA silica are schematically illustrated in Figure 6c. Previously, immobilization of biomaterials such as protein or enzymes over the composite addressed the higher enzyme activity compared to that of free enzyme.[45] However, after reaching the critical immobilized concentration of the enzyme, the efficiency of the enzyme can be rapidly decreased owing to improper distortion of α helix structure.[46] Therefore, the proper adsorption of polymerase could modulate its activity and provide the binding sites to the PCR reagents to improve their stability during the PCR. Moreover, the unique chemical structural properties and high surface area of nanocomposite may help to increase dispersibility of nanocomposites and stability of both primers and polymerase during PCR.[47,48] These balances of binding capability of polymerase, primers, silica, and PDA as well as the carbonization of PDA gave the synergetic effect and best condition to enhance the PCR efficiency.

Additionally, the PCR enhancement could be understood from melting temperature changes of DNA as corresponding to the nanocomposites (Figure S3 in the Supporting Information). The positive control sample without using nanocomposites) showed the melting curve at 76 °C (gray line from Supporting Information Figure S3). With the introduction of silica, PDA silica, and C-PDA silica, the melting curves via temperatures of the PCR products were slightly increased and presented a single peak at 79.5 °C (red, blue, and green lines in Supporting Information Figure S3). As compared to the positive control, the melting temperature changes were mainly attributed to the stability enhancement of PCR reagents over the nanocomposites. These phenomena also indicated that nanocomposites prohibited the primer−dimer and minimized mispriming of target sequences.

4. CONCLUSIONS

In summary, we have reported a simple, biocompatible, and green chemical way to synthesize carbon-coated silica using PDA as a bioadhesive and carbon source. The subsequential thermal carbonization of PDA converted the disordered PDA into ordered carbon structures which are similar to the graphitic structures. We also directly observed the effects of C-PDA silica in PCR by employing as-prepared silica and PDA silica to investigate the interaction between the materials and PCR reagents in PCR. The strong negative charges of silica showed almost no interaction with primers and polymerase. By contrast, the PDA silica provided numerous binding sites to immobilize the primers and polymers on the surface to enhance their stability. Moreover, C-PDA silica allowed for mild interaction with primers and polymerase but addressed the best PCR enhancement among them. These observations suggested that the combination of silica, PDA, and carbonization enables one to make a harmony condition to influence the PCR reagents and contributed to the PCR enhancement. The different characteristics of nanocomposites facilitate a unique environment and diverse conditions to interact with PCR reagents. Therefore, these findings could provide new

insight for understanding the PCR effects of composite materials and their mechanism study. Moreover, these materials will be valuable for future applications in biomedical, diagnostic, and biosensing applications.

■ ASSOCIATED CONTENT

Ⓢ Supporting Information
SEM image of silica particles, element mapping of both silica and PDA silica, and melting temperature changes of DNA. The Supporting Information is available free of charge on the ACS Publications website at DOI: 10.1021/acsami.5b04404.

■ AUTHOR INFORMATION

Corresponding Authors
*(K.G.L.) Tel.: +82 42 366 1914. Fax: +82 42 366 1990. E-mail: kglee@nnfc.re.kr.
*(T.J.P.) Tel.: +82 2 820 5220. Fax: +82 2 825 4736. E-mail: tjpark@cau.ac.kr.

Notes
The authors declare no competing financial interest.

■ ACKNOWLEDGMENTS

■ REFERENCES

(1) Yang, L.; Du, F.; Chen, G.; Yasmeen, A.; Tang, Z. A Novel Colorimetric PCR-Based Biosensor for Detection and Quantification of Hepatitis B Virus. *Anal. Chim. Acta* **2014**, *840*, 75−81.

(2) Wang, G.; Wormser, G. P.; Zhuge, J.; Villafuerte, P.; Ip, D.; Zeren, C.; Fallon, J. T. Utilization of A Real-Time PCR Assay for Diagnosis of Babesia Microti Infection in Clinical Practice. *Ticks Tick-Borne Dis.* **2015**, *6*, 376−382.

(3) Lazcka, O.; Campo, F. J. D.; Munoz, F. X. Pathogen Detection: A Perspective of Traditional Methods and Biosensors. *Biosens. Bioelectron.* **2007**, *22* (7), 1205−1217.

(4) Clark, T. A.; Murray, L. A.; Morgan, R. D.; Kislyuk, A. O.; Spittle, K. E.; Boitano, M.; Fomenkov, A.; Roberts, R. J.; Korlach, J. Characterization of DNA Methyltransferase Specificities Using Single-Molecule, Real-Time DNA Sequencing. *Nucleic Acids Res.* **2012**, *40*, e29.

(5) Chen, P.; Pan, D.; Fan, C.; Chen, J.; Huang, K.; Wang, D.; Zhang, H.; Li, Y.; Feng, G.; Liang, P.; He, L.; Shi, Y. Gold Nanoparticles for High-Throughput Genotyping of Long-range Haplotypes. *Nat. Nanotechnol.* **2011**, *6*, 639−644.

(6) Pérez-Pérez, F. J.; Hanson, N. D. Detection of Plasmid-Mediated AmpC β-Lactamase Genes in Clinical Isolates by Using Multiplex PCR. *J. Clin. Microbiol.* **2002**, *40*, 2153−2162.

(7) Garibyan, L.; Avashia, N. Research Techniques Made Simple: Polymerase Chain Reaction (PCR). *J. Invest. Dermatol.* **2013**, *133*, e6.

(8) Acinas, S. G.; Sarma-Rupavtarm, R.; Klepac-Ceraj, V.; Polz, M. F. PCR-Induced Sequence Artifacts and Bias: Insights from Comparison of Two 16S rRNA Clone Libraries Constructed from the Same Sample. *Appl. Environ. Microbiol.* **2005**, *71*, 8966−8969.

(9) Yuce, M.; Kurt, H.; Mokkapati, V. R. S. S.; Budak, H. Employment of Nanomaterials in Polymerase Chain Reaction: Insight into the Impacts and Putative Operating Mechanisms of Nano-Additives in PCR. *RSC Adv.* **2014**, *4*, 36800−36814.

(10) Li, H.; Huang, J.; Lv, J.; An, H.; Zhang, X.; Zhang, Z.; Fan, C.; Hu, J. Nanoparticle PCR: Nanogold-Assisted PCR with Enhanced Specificity. *Angew. Chem., Int. Ed.* **2005**, *44*, 5100−5103.

(11) Li, M.; Lin, Y.-C.; Wu, C.-C.; Liu, H. -. Enhancing the Efficiency of A PCR Using Gold Nanoparticles. *Nucleic Acids Res.* **2005**, *33*, e184.

(12) Liang, G.; Ma, C.; Zhu, Y.; Li, S.; Shao, Y.; Wang, Y.; Xiao, Z. Enhanced Specificity of Multiplex Polymerase Chain Reaction via CdTe Quantum Dots. *Nanoscale Res. Lett.* **2010**, *6*, 51.

(13) Wang, L.; Zhu, Y.; Jiang, Y.; Qiao, R.; Zhu, S.; Chen, W.; Xu, C. Effects of Quantum Dots in Polymerase Chain Reaction. *J. Phys. Chem. B* **2009**, *113*, 7637−7641.

(14) Liang, Y.; Luo, F.; Lin, Y.; Zhou, Q. F.; Jiang, G. B. C60 Affects DNA Replication in Vitro by Decreasing the Melting Temperature of DNA Templates. *Carbon* **2009**, *47*, 1457−1465.

(15) R, A. K.; Kafafy, R.; Salleh, H. M.; Faris, W. F. Enhancing the Efficiency of Polymerase Chain Reaction Using Graphene Nanoflakes. *Nanotechnology* **2012**, *23*, 455106−455114.

(16) Jia, J.; Sun, L.; Hu, N.; Huang, H.; Weng, J. Graphene Enhances the Specificity of the Polymerase Chain Reaction. *Small* **2012**, *8*, 2011−2015.

(17) Yuce, M.; Budak, H. Dispersion Quality of Amine Functionalized Multiwall Carbon Nanotubes Plays Critical Roles in Polymerase Chain Reaction Enhancement. *J. Nanopart. Res.* **2014**, *16*, 2768.

(18) Zhang, Z.; Shen, C.; Wang, M.; Han, H.; Cao, X. Aqueous Suspension of Carbon Nanotubes Enhances the Specificity of Long PCR. *BioTechniques* **2008**, *44*, 537−545.

(19) Williams, R. M.; Nayeem, S.; Dolash, B. D.; Sooter, L. J. The Effect of DNA-Dispersed Single-Walled Carbon Nanotubes on the Polymerase Chain Reaction. *PLoS One* **2014**, *9*, e94117.

(20) R, A. K.; Sonawane, P. J.; Sasi, B. K.; Sahu, B. S.; Pradeep, T.; Das, K. S.; Mahapatra, N. R. Enhancement in the Efficiency of Polymerase Chain Reaction by TiO2 Nanoparticles: Crucial Role of Enhanced Thermal Conductivity. *Nanotechnology* **2010**, *21*, 255704.

(21) Wang, X. Q.; Mujumdar, A. S. Heat Transfer Characteristics of Nanofluids: A Review. *Int. J. Therm. Sci.* **2007**, *46*, 1−19.

(22) Balandin, A. A.; Ghosh, S.; Bao, W.; Calizo, I.; Teweldebrhan, D.; Miao, F.; Lau, C. N. Superior Thermal Conductivity of Single-Layer Graphene. *Nano Lett.* **2008**, *8*, 902−907.

(23) Hone, J.; Llaguno, M. C.; Biercuk, M. J.; Johnson, A. T.; Batlogg, B.; Benes, Z.; Fischer, J. E. Thermal Properties of Carbon Nanotubes and Nanotube-Based Materials. *Appl. Phys. A: Mater. Sci. Process.* **2002**, *74*, 339−343.

(24) Varghese, N.; Mogera, U.; Govindaraj, A.; Das, A.; Maiti, P. K.; Sood, A. K.; Rao, C. N. R. Binding of DNA Nucleobases and Nucleosides with Graphene. *ChemPhysChem* **2009**, *10*, 206−210.

(25) Tu, X.; Manohar, S.; Jagota, A.; Zheng, M. DNA Sequence Motifs for Structure-Specific Recognition and Separation of Carbon Nanotubes. *Nature* **2009**, *460*, 250−253.

(26) Allen, M. J.; Tung, V. C.; Kaner, R. B. Honeycomb Carbon: A Review of Graphene. *Chem. Rev.* **2010**, *110*, 132−145.

(27) Li, X.; Chen, Y.; Mo, S.; Jia, L.; Shao, X. Effect of Surface Modification on the Stability and Thermal Conductivity of Water-Based SiO2-Coated Graphene Nanofluid. *Thermochim. Acta* **2014**, *595*, 6−10.

(28) Tan, W.; Wang, K.; He, X.; Zhao, X. J.; Drake, T.; Wang, L.; Bagwe, R. P. Bionanotechnology Based on Silica Nanoparticles. *Med. Res. Rev.* **2004**, *24*, 621−638.

(29) Sanchez, C.; Julián, B.; Belleville, P.; Popall, M. Applications of Hybrid Organic−Inorganic Nanocomposites. *J. Mater. Chem.* **2005**, *15*, 3559−3592.

(30) Zou, H.; Wu, S.; Shen, J. Polymer/Silica Nanocomposites: Preparation, Characterization, Properties, and Applications. *Chem. Rev.* **2008**, *108*, 3893−3957.

(31) Lee, H. S.; Dellatore, S. M.; Miller, W. M.; Messersmith, P. B. Mussel-Inspired Surface Chemistry for Multifunctional Coatings. *Science* **2007**, *318*, 426−430.

(32) Lynge, M. E.; van der Westen, R.; Postma, A.; Stadler, B. Polydopamine-A Nature-Inspired Polymer Coating for Biomedical Science. *Nanoscale* **2011**, *3*, 4916−4928.

(33) Seok, S. H.; Choi, I. S.; Lee, G. K.; Choi, B. K.; Park, K. J.; Park, J. Y.; Kwon, O. J.; Lee, S. J.; Kim, D. H. Dopamine-Induced Pt and N-doped Carbon@Silica Hybrids as High-Performance Anode Catalysts for Polymer Electrolyte Membrane Fuel Cells. *RSC Adv.* **2014**, *4*, 42582−42584.

(34) Lei, C.; Han, F.; Li, D.; Li, W. C.; Sun, Q.; Zhang, X. Q.; Lu, A. H. Dopamine as the Coating Agent and Carbon Precursor for the Fabrication of N-doped Carbon Coated Fe3O4 Composites as Superior Lithium Ion Anodes. *Nanoscale* **2013**, *5*, 1168−1175.

(35) Kong, J.; Yee, W.A.; Yang, L.; Wei, Y.; Phua, S. L.; Ong, H. G.; Ang, J. M.; Li, X.; Lu, X. Highly Electrically Conductive Layered Carbon Derived from Polydopamine and its Functions in SnO2-Based Lithium Ion Battery Anodes. *Chem. Commun.* **2012**, *48*, 10316−10318.

(36) Yu, X.; Fan, H.; Liu, Y.; Shi, Z.; Jin, Z. Characterization of Carbonized Polydopamine Nanoparticles Suggests Ordered Supramolecular Structure of Polydopamine. *Langmuir* **2014**, *30*, 5497−5505.

(37) Sugimoto, T. Preparation of Monodispersed Colloidal Particles. *Adv. Colloid Interface Sci.* **1987**, *28*, 65−108.

(38) Putz, A. M.; Putz, M. V. Spectral Inverse Quantum (spectral-IQ) Method for Modeling Mesoporous Systems: Application on Silica Films by FTIR. *Int. J. Mol. Sci.* **2012**, *13*, 15925−15941.

(39) Morrow, B. A.; McFarlan, A. J. Surface Vibrational Modes of Silanol Groups on Silica. *J. Phys. Chem.* **1992**, *96*, 1395−1400.

(40) Centeno, S. A.; Shamir, J. Surface Enhanced Raman Scattering (SERS) and FTIR Characterization of the Sepia Melanin Pigment used in Works of Art. *J. Mol. Struct.* **2008**, *873*, 149−159.

(41) Ferrari, A. C. Raman Spectroscopy of Graphene and Graphite: Disorder, Electron−Phonon Coupling, Doping and Nonadiabatic Effects. *Solid State Commun.* **2007**, *143*, 47−57.

(42) Gao, W.; Alemany, L. B.; Ci, L.; Ajayan, P. M. New Insights into the Structure and Reduction of Graphite Oxide. *Nat. Chem.* **2009**, *1*, 403−408.

(43) Eckmann, A.; Felten, A.; Verzhbitskiy, I.; Davey, R.; Casiraghi, C. Raman Study on Defective Graphene: Effect of the Excitation Energy, Type, and Amount of Defects. *Phys. Rev. B: Condens. Matter Mater. Phys.* **2013**, *88*, 035426.

(44) Ferrari, A. C.; Meyer, J. C.; Scardaci, V.; Casiraghi, C.; Lazzeri, M.; Mauri, F.; Piscanec, S.; Jiang, D.; Novoselov, K. S.; Roth, S.; Geim, A. K. Raman Spectrum of Graphene and Graphene Layers. *Phys. Rev. Lett.* **2006**, *97*, 187401.

(45) Singh, R. K.; Tiwari, M. K.; Singh, R.; Lee, J. K. Protein Engineering to Immobilization: Promising Strategies for the Upgrade of Industrial Enzymes. *Int. J. Mol. Sci.* **2013**, *14*, 1232−1277.

(46) Asuri, P.; Bale, S. S.; Karajanagi, S. S.; Kane, R. S. The Protein−Nanomaterial Interface. *Curr. Opin. Biotechnol.* **2006**, *17*, 562−568.

(47) Mi, L.; Wen, Y.; Pan, P.; Wang, Y.; Fan, C.; Hu, J. Modulation of DNA Polymerases with Gold Nanoparticles and their Applications in Hot-Start PCR. *Small* **2009**, *5*, 2597−2600.

(48) Vu, B. V.; Litvinov, D.; Willson, R. C. Gold Nanoparticle Effects in Polymerase Chain Reaction: Favoring of Smaller Products by Polymerase Adsorption. *Anal. Chem.* **2008**, *80*, 5462−5467.

■ NOTE ADDED AFTER ASAP PUBLICATION

This paper was published ASAP on July 7, 2015, with an incorrect Figure 5. The corrected paper was reposted on July 9, 2015.